International Journal of Microwave and Wireless Technologies

cambridge.org/mrf

Design of a hybrid A-sandwich radome using a strongly coupled frequency selective surface element

Krushna Kanth Varikuntla and Raghavan Singaravelu

Department of Electronics and Communication Engineering, National Institute of Technology Tiruchirappalli, Trichy, India

Research Paper

Cite this article: Varikuntla KK, Singaravelu R (2020). Design of a hybrid A-sandwich radome using a strongly coupled frequency selective surface element. *International Journal of Microwave and Wireless Technologies* **12**, 738–748. https://doi.org/10.1017/S1759078720000021

Received: 12 September 2019
Revised: 27 December 2019
Accepted: 8 January 2020
First published online: 10 February 2020

Keywords:
EM field theory and numerical techniques; multi-layer; radome; strongly coupled-frequency selective surfaces microwave measurements; wave propagation and scattering: modeling and measurements

Author for correspondence:
Krushna Kanth Varikuntla, E-mail: krushnakanthv@gmail.com

Abstract

The airborne radomes have to cater superior electromagnetic (EM) performance with bandpass characteristics of stealth application. In this regard, a hybrid A-sandwich radome is proposed in this paper. The proposed radome consists of a novel strongly coupled frequency selective surface (FSS) core sandwiched between two dielectric layers (acts as skin) to form an A-sandwich structure. The dielectric layers are cascaded in such a way that the middle layer has less dielectric parameters than the skin dielectric. The core layer comprises a modified FSS array using strongly coupled FSS layers through a series of metallic vias. This strongly-coupled FSS element will have the advantage of eliminating inter-element interference and improves the EM performance characteristics of the structure. The structure exhibits very good band-pass characteristics (>90%) at a normal impinging angle with sharp roll-off characteristics. To show the efficacy of the proposed structure, the transmission loss has been compared with that of conventional A-sandwich radomes at 0°, 50° incidence angle for both TE and TM polarization. Conformal analysis of the unit cell has been carried out, and sector-wise thickness optimization was performed to analyze the structure for the conformal shaped radome application. Finally, a physical prototype has been fabricated and measured its scattering parameters, radiation characteristics in a fully shielded anechoic chamber. The results are encouraging and prove its suitability for radome application.

Introduction

Aircraft/missiles and surface vehicle radomes are classified by specific wall structure and used in aerospace applications. Over the band of frequencies, high transmission efficiency, low radar cross-section (RCS), and minimum boresight error are more desirable performance characteristics of modern radomes [1, 2]. The superior electromagnetic (EM) performance, structural and environmental stability is the major challenge in the design of radome [3]. Advancements in modern radar systems lead to the demand for novel EM design techniques to meet the desired radome performance. In recent years, rapid growth in the fields of EM design and analysis techniques based on advanced numerical computations and hybrid algorithms [4, 5]. Many EM design techniques have been reported to cater the desired performance of radome structures [6–9]. Frequency selective surfaces (FSSs) are the planar, periodic structure, and may be printed on a substrate or a conducting screen perforated with slots to exhibit filter characteristics for EM waves impinge on it [10]. The FSSs can be used in the design of spatial filters, radar absorbing structure, radome, and high impedance surfaces [11]. From the past few decades, these FSS structures have been widely used in various aerospace, wireless communication, and in high-power microwave systems. A common application of FSS involves in the design of radome that protects an antenna from atmospheric conditions and impacts the EM performance of the antenna as little as possible in the operating band [4, 5]. In General, radomes are typically constructed from high strength materials opt for the application, with metalized FSSs embedded within the chosen materials [3]. The radome being in the near vicinity of the antenna, mutual interactions of the antenna and FSS screen complicate the design.

Initially, FSS-based radomes were designed for a flat band-pass response and sharp roll-off characteristics outside the band [10]. Later on, various types of FSS-based radomes such as monolithic, A-sandwich, and multilayered were designed for broadband and low RCS applications [12, 13]. Since the conventional radomes suffer from poor performance at higher incident angles, the FSS based will be a better choice for aerospace applications. The basic FSS radome design consists of a band-pass FSS array made of apertures, buried in a conventional dielectric substrate. In monolithic radome, the FSS array can be inserted into the mid-plane wall of the substrate. In multilayered walls such as A-, C-sandwiched structures, FSS usually buried in the core layer. Another way of designing FSS based radome is cascading two

© Cambridge University Press and the European Microwave Association 2020

CAMBRIDGE UNIVERSITY PRESS

thick FSS layers separated by a dielectric substrate. Nevertheless, the performance of FSS degrades in the millimeter-wave frequency range [14]. To overcome the demerits of these conventional FSS elements, metamaterial (MTM)-based FSS elements have been proposed in the open literature. However, MTM elements show unusual material characteristics in different frequency regions which are difficult to achieve.

The present paper deals with the design of a hybrid A-sandwich radome wall using strongly coupled FSS based on vias technology for the aerospace applications. The design comprises two symmetrical FSS arrays printed on either side of the substrate and strongly coupled through a series of metallic vias. The modified FSS structure with metallic posts partially results in the usage of substrate integrated waveguide (SIW) technology for patch type FSS. Each element of the proposed FSS is configured as a resonant reactive impedance surface. The proposed FSS structure resembles the advantages of a waveguide structure with a high-quality factor [15–17]. The details design methodology, EM performance analysis and characteristics of the closely coupled FSS element have been discussed in our previous publication [18]. In this paper, the advantage of the proposed element for radome application has been presented. The different design considerations for radome and optimizations have been analyzed in detail.

Further, to model the A-sandwich radome, the proposed FSS structure is buried in between two dielectric layers (dielectric skin). Since the structure uses novel strongly coupled FSS elements, the radome structure has been named as a hybrid A-sandwich radome. The FSS elements exhibit stopband characteristics at the first resonance, whereas the second higher-order stopband is obtained from the frequency selective properties of dielectric layers with a very stable performance. The pass-band between two reflection bands is used to operate the radome with reduced out band RCS. Also, the frequency tuning can be achieved by adjusting the FSS design parameters. To show the efficacy of the proposed configurations, the EM performance is compared with that of conventional A-sandwich radome given in [3].

EM design considerations of hybrid A-sandwich radome wall

An A-sandwich radome structure is comprised two dielectric skin layers of the higher dielectric constant separated by a core having a lower dielectric constant than the skins [3]. The radome structure with dielectric layers is shown in Fig. 1. The structural representation of conventional A-sandwich, A-sandwich embedded with FSS and proposed A-sandwich embedded with strongly coupled FSS is shown in Figs. 1(a)–1(c) respectively. Initially, to understand the behavior of an A-sandwich radome, a conventional structure is designed. The general construction of the inhomogeneous radome wall is shown in Fig. 2(a). The number of dielectric layers (N) of the design is 3 for an A-sandwich radome. The design parameters of conventional A-sandwich structure are: thickness of top and bottom skins is $t_1 = t_3 =$ 0.762 mm respectively, dielectric constant $\varepsilon_r = 3.35$, and loss tangent $\tan\delta = 0.016$. A low profile dielectric foam has been considered as a core (dielectric constant 1.1, $\tan\delta = 0.001$) with thickness $t_2 = 10.16$ mm [3]. The transmission loss performance characteristics of the wall have been studied in the frequency range from 0 to 25 GHz for the normal incident angle using the transmission parameter (ABCD parameters) method [19].

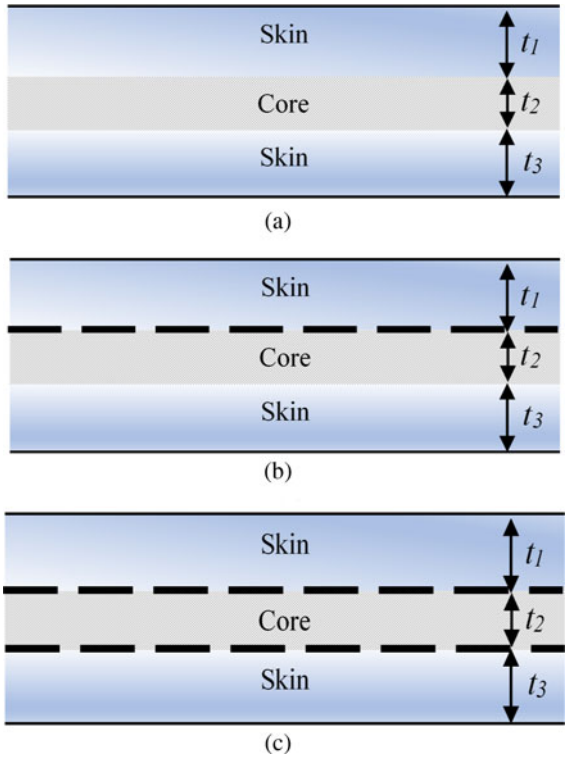


Fig. 1. Composition of the radome wall: (a) A-sandwich, (b) embedded with single layer FSS array, and (c) embodiment structure with the modified FSS array.

The transmission parameters of an FSS element can be modeled as a parallel admittance (Y_{FSS}) network [20]. The admittance of the proposed FSS radome can be computed based on their equivalent circuit model (ECM) shown in Fig. 2(b). Where Y_1 and Y_2 are the admittance offered by the patch FSS elements printed on either side of the substrate ($Y_1 = Y_2 = Y_{FSS}$) [23]. Whereas Y_3 is the admittance offered by the metallic vias connected two FSS arrays through the dielectric substrate.

$$Y_3 = j\left(\frac{\omega L_{via}}{n} - \frac{1}{\omega C_{via}}\right)^{-1} \quad (1)$$

L_{via} and C_{via} are the lumped elements formed by the metallic vias through the substrate and they are connected in parallel. In the expression, n represents the number of vias in one unit cell and ω is the resonance frequency. The inductance (L_{via}) can be computed from equation (2) [28].

$$L_{via} = 2h\left\{\ln\left[\left(\frac{1+\sqrt{1+a^2}}{a}\right)\right] - \sqrt{1+R^2} + \frac{\mu}{4} + a\right\} nH \quad (2)$$

where $a = \frac{D}{2h}$, $R = \sqrt{1+a^2}$, D and h are the diameter and length of the metallic vias (height of the substrate). The numerical value of via inductance computed with equation (2) is $L_{via} = 0.724$ mH and the capacitance value is $C_{via} = 2.39$ pF which is computed using the relation $\varepsilon A/h$. Where A is the plate area. Z_s and Z_0 are

https://doi.org/10.1017/S1759078720000021 Published online by Cambridge University Press

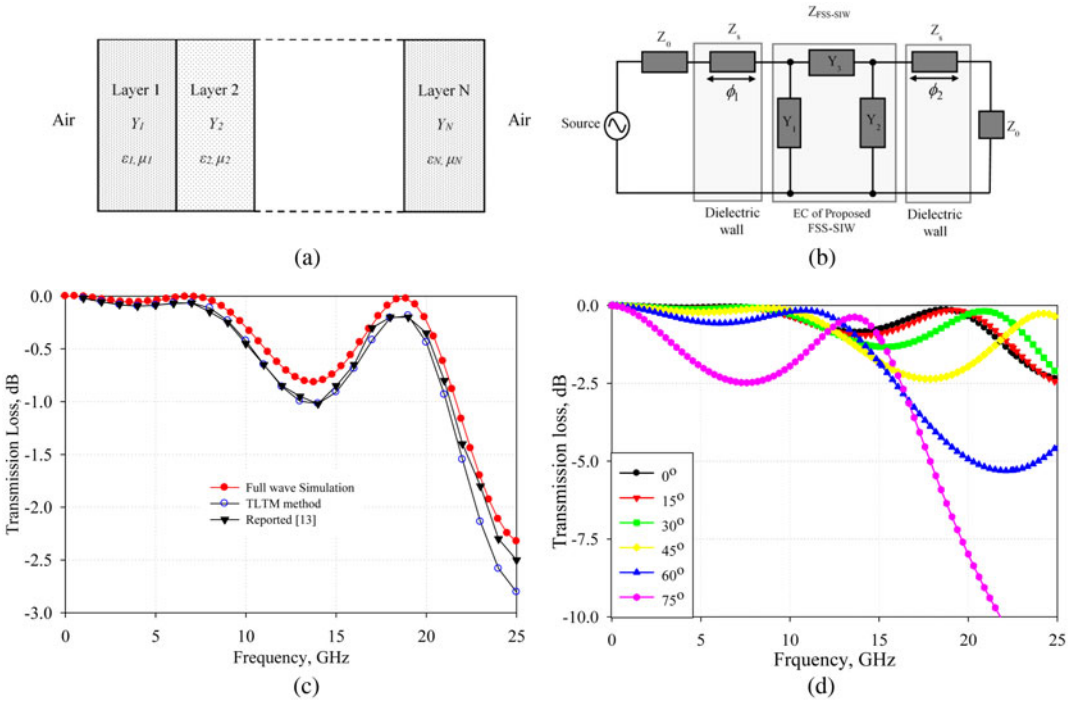


Fig. 2. Transmission line model analysis: (a) dielectric wall construction of the inhomogeneous radome wall, (b) equivalent model of the proposed radome wall, (c) transmission loss performance of the conventional A-sandwich radome wall at the normal incident angle, and (d) oblique incidence angle.

the impedance offered by the dielectric skin and air respectively.

$$\begin{bmatrix} A_i & B_i \\ C_i & D_i \end{bmatrix} = \begin{bmatrix} \cos\varphi_i & \dfrac{j\sin\varphi_i}{Y_{ci}} \\ jY_{ci}\sin\varphi_i & \cos\varphi_i \end{bmatrix};\ i = 1.2.3\ldots N \quad (3)$$

where $Y_{ci}$is the ratio of admittance of the ith medium to $(i+1)$st medium, ϕ_i is the electrical length of the ith layer which depends on the thickness and dielectric constant of the substrate, and N denotes the number of layers.

The total transmission parameters of the structure are equivalent to the matrix multiplication of individual layer parameters, which can be expressed as:

$$\begin{bmatrix} A & B \\ C & D \end{bmatrix} = \begin{bmatrix} A_1 & B_1 \\ C_1 & D_1 \end{bmatrix} \cdot \begin{bmatrix} A_2 & B_2 \\ C_2 & D_2 \end{bmatrix} \cdots \begin{bmatrix} A_N & B_N \\ C_N & D_N \end{bmatrix} \quad (4)$$

Finally, the transmission coefficient of the structure is given as:

$$T = \frac{2}{A + B + C + D} \quad (5)$$

Equation (5) can compute the transmission parameters of the structure.

The same method can be used to analyze the transmission response of the FSS based radome wall. The transmission matrix of the proposed FSS is:

$$\begin{bmatrix} A_{FSS} & B_{FSS} \\ C_{FSS} & D_{FSS} \end{bmatrix} = \begin{bmatrix} 1 & 0 \\ \dfrac{1}{Z_{FSS}} & 1 \end{bmatrix} \quad (6)$$

In the above equation, $Z_{FSS-SIW}$ is the impedance offered by the proposed strongly coupled FSS. Finally, the transmission parameters of the proposed structure are:

$$\begin{bmatrix} A & B \\ C & D \end{bmatrix} = \begin{bmatrix} A_1 & B_1 \\ C_1 & D_1 \end{bmatrix} \cdot \begin{bmatrix} A_{FSS} & B_{FSS} \\ C_{FSS} & D_{FSS} \end{bmatrix} \cdot \begin{bmatrix} A_2 & B_2 \\ C_2 & D_2 \end{bmatrix} \quad (7)$$

This method is capable of computing transmission, reflection, and absorption coefficients of multi-layered structures at an oblique angle of incidence for both parallel (TE) and perpendicular (TM) polarizations. The transmission loss performance of the conventional A-sandwich radome wall structure is analyzed by this method as per equations (3)–(5). The results obtained by this method are compared with that of the reported results [3] and finite difference time domain based full-wave commercial simulator (CST MWS). The comparison of results at normal incidence is shown in Fig. 2(c). The simulated results for oblique incidence are shown in Fig. 2(d). The results obtained based on the ABCD parameter method (or transmission line model) and full-wave simulation are good in agreement with the reported results from [3]. Hence, the transmission line model is the easiest and fast method to estimate the basic performance of a multilayered radome wall. Further, full-wave simulations can be used for final optimal design. The performance of the proposed hybrid radome wall has been analyzed by appending the FSS in a conventional form and proposed coupled-FSS form using CST MWS. The thickness and dielectric profile of the proposed structure have given in Table 1. The unit cell boundary conditions along x-, y-, and open boundary conditions along the z-direction have been applied respectively for Floquet mode analysis. The effect of anti-static, anti-erosion paint ($\varepsilon_r = 3.46$, loss tangent $\tan\delta = 0.068$ and thickness = 0.2 mm) coated on outermost surfaces of

https://doi.org/10.1017/S1759078720000021 Published online by Cambridge University Press

Table 1. Thickness profile of the radome wall.

Layer no.	1	2	3
Thickness (mm)	2.0	0.81	2.0
Dielectric constant	4.3	3.28	4.3
Loss tangent	0.025	0.002	0.025

the structure is also taken into account to cater the practical scenario. Hence, the total optimized thickness of the wall is found to be 5.21 mm. The proposed design resembles the reinforced metallic structure, which increases the physical strength of the radome wall compared to the multilayered dielectric walls at low thickness.

Design aspects of strongly coupled FSS element

A metallic cage structure can be developed around the sensitive portions of an integrated circuit in a system, to protect/suppress interference from neighboring circuits [21, 22]. The working principle of the design is, when an external field applied to the cage, electrons in metal displaces, results in negative charge accumulate at one side, whereas positive charge will develop at another side. This induced-electrical polarization cancels out the external electric field, which makes the structure to exhibit angularly stable performance. The same technique is used here to design polarization-independent FSS elements with improved bandwidth. In this work, the basic element used in FSS analysis such as Jerusalem cross (JC) [23] is investigated. The SIW vias technology has been applied to this element to create proposed structural topology. The patch type JC FSS element is designed at 10 GHz, center frequency of the X-band. The unit cell configuration of JC FSS in its conventional form as well its modified form is shown in Figs. 3(a)–3(c) respectively.

Design of Jerusalem cross element

JC FSS is a cross element which consists of a pair of loaded dipoles at the end of arms. The loaded dipoles will increase the end capacitance. The same element has been considered for designing the strongly coupled FSS based on vias technology. The patch type JC is printed on either side of a dielectric substrate and strongly coupled through metallic vias. The optimized structural dimensions of JC are: $p = 9.25$ mm which corresponds to $\approx 0.3\lambda_0$ (λ_0 is the wavelength at center frequency), arm length of JC $d = 2.3$ mm, and the width of JC cross and arm are $w = t = 0.65$ mm. The design parameters of the post are: diameter $D = 0.5$ mm and spacing between neighboring posts is maintained to avoid the EM leakage through the structure which is $K = 0.635$ mm.

The necessary conditions to design metallic posts are considered from [24]. A dielectric material with $\varepsilon_r = 3.38$, loss tangent $\tan\delta = 0.0027$ has been used as a substrate. The initial design parameters of FSS elements are computed from its ECM [23]. Then, the fine designs have been developed using full-wave simulations.

The metallic vias will act as series inductance (L) between two parallel LC networks (equivalent circuit of FSS). The EM performance characteristics of the proposed FSS element have been compared with its own conventional form which is shown in Fig. 3(d). The modified FSS elements exhibit a considerable improvement in their stop-band. In the modified FSS element, the bandwidth (−10 dB) has been improved significantly. In the case of JC element is from 1.9 GHz (8.9–10.8 GHz) to 3.07 GHz (8.43–11.5 GHz), offers an improvement of 11.52% than in its conventional form, which covers the entire X-band region. However, the vias diameter and spacing have a minor contribution to frequency response which cannot be ignored. The necessary conditions $D/k \geq 0.5$ and $D/\lambda_0 \leq 0.1$ are maintained to form the vias cage [24]. The initial values of the via parameter are computed using the relation as follows:

$$k < \frac{\lambda_0\sqrt{\varepsilon_r}}{2} \text{ and } k < 4D \tag{8}$$

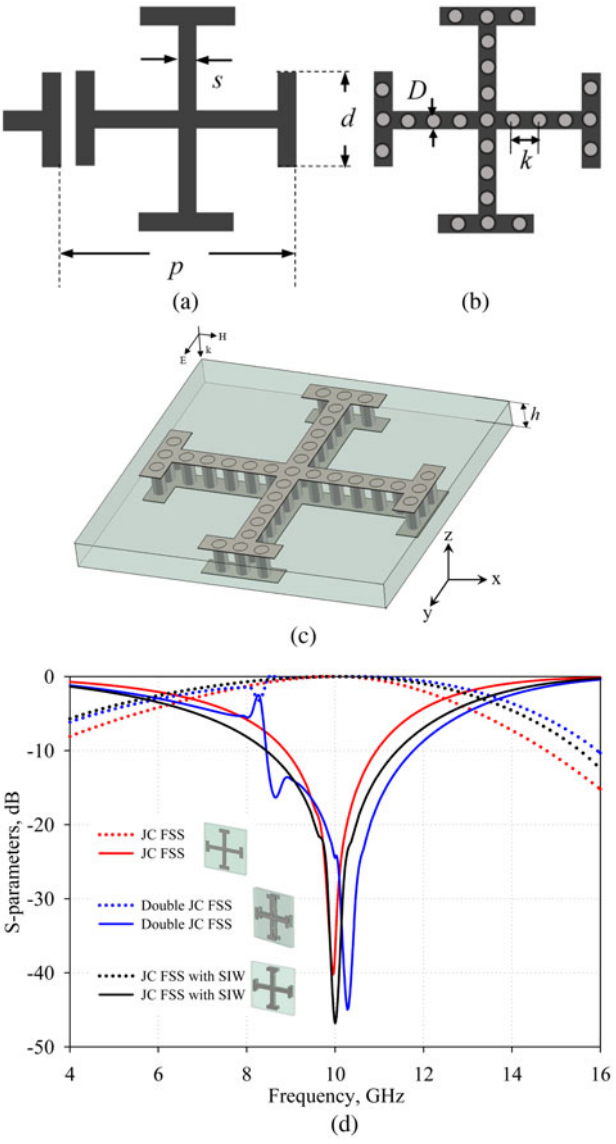


Fig. 3. Design of the FSS unit cell. (a) Conventional JC, (b) JC with SIW technology, (c) perspective view of the proposed unit cell, and (d) transmission and reflection characteristics of conventional (red), double-layered (blue), and proposed FSS (black). The solid line shows the transmission coefficient and the dotted line shows the reflection coefficient.

https://doi.org/10.1017/S1759078720000021 Published online by Cambridge University Press

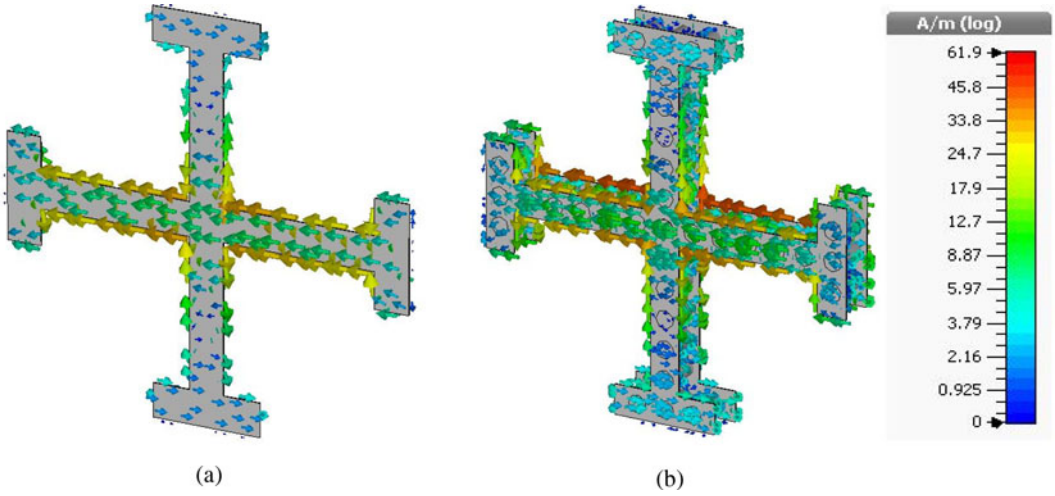


Fig. 4. Surface current distribution at 10 GHz on: (a) JC FSS and (b) proposed JC.

Table 2. Effect of the incident angle on the resonance performance of JC.

	Single layer JC FSS			Strongly coupled JC FSS		
Angle of incidence (°)	Resonance frequency (in GHz)	Deviation (in %)	10 dB FBW (in %)	Resonance frequency (in GHz)	Deviation (in %)	10 dB FBW (in %)
0	10.0	0	20.2	10.0	0	30.0
10	9.90	−1.0	20.94	10.0	0	30.3
20	9.92	−0.8	21.54	10.0	0	30.71
30	9.88	−1.2	23.6	10.0	0	31.47
40	9.81	−1.9	24.97	9.87	−1.3	37.75
50	9.74	−2.6	30.9	9.80	−2.0	41.93
60	9.70	−3.0	37.42	9.75	−2.5	54.34
70	9.63	−3.7	52.37	9.72	−2.8	67.40

where D corresponds the diameter of the metallic vias, k for their distance respectively. λ_0 represents the wavelength at the operating frequency and ε_r is the relative permittivity of the dielectric substrate. Apart from the wider bandwidth, the proposed structure offers high power handling capabilities [25, 26] and structural strength when used as a reinforced structure. Figures 4(a) and 4(b) showed the uniformly distributed strong surface currents on conventional FSS and proposed FSS at 10 GHz respectively when a plane-wave incident on it normally. At the resonance frequency, strong fields are found in the proposed structure than in its conventional form. Also, the conventional FSS elements are suffered to show their basic performance characteristics at high power levels [27, 28]. The proposed structural topology can be able to exhibit its basic performance characteristics even at high power levels because of the virtually thick surface. It is believed that coupling of patch type FSS elements using vias technology is used for the first time for the design of the radome wall configuration with very good band-pass characteristics. Table 2 shows the dependency of the incidence angle on the resonance characteristics of the proposed structure. The bandwidth shown in Table 2 is the stopband bandwidth. As the stopband increases, the out-of-band rejection improves in the radome design.

Design and performance analysis of hybrid A-sandwich radome

Radomes are installed over the radar and antenna system to protect them from environmental effects, which are also electromagnetically transparent and act as a band-pass filter. The structure allows the operating frequencies with least insertion loss and rejects all-out band frequencies. Thus, they tend to reduce the RCS of the antenna. The structure should furnish an appropriate response for the impinging EM waves in a specified frequency band and range of incident angles. The first resonance at a lower frequency is occurred due to the metallic coupled-FSS element. Whereas, the dielectric substrate is responsible for the higher-order resonance. The design frequency of the proposed FSS elements is shifted to a lower frequency by a factor of $\sqrt{\varepsilon_r}$, and resonance may found in between f_0 and $f_0/\sqrt{\varepsilon_r}$. Here, the stopband is found at 6.85 GHz from 10 GHz. This results in sharp roll-off performance at lower frequencies and a flat transmission response from 8.5 GHz with greater than 90% efficiency.

https://doi.org/10.1017/S1759078720000021 Published online by Cambridge University Press

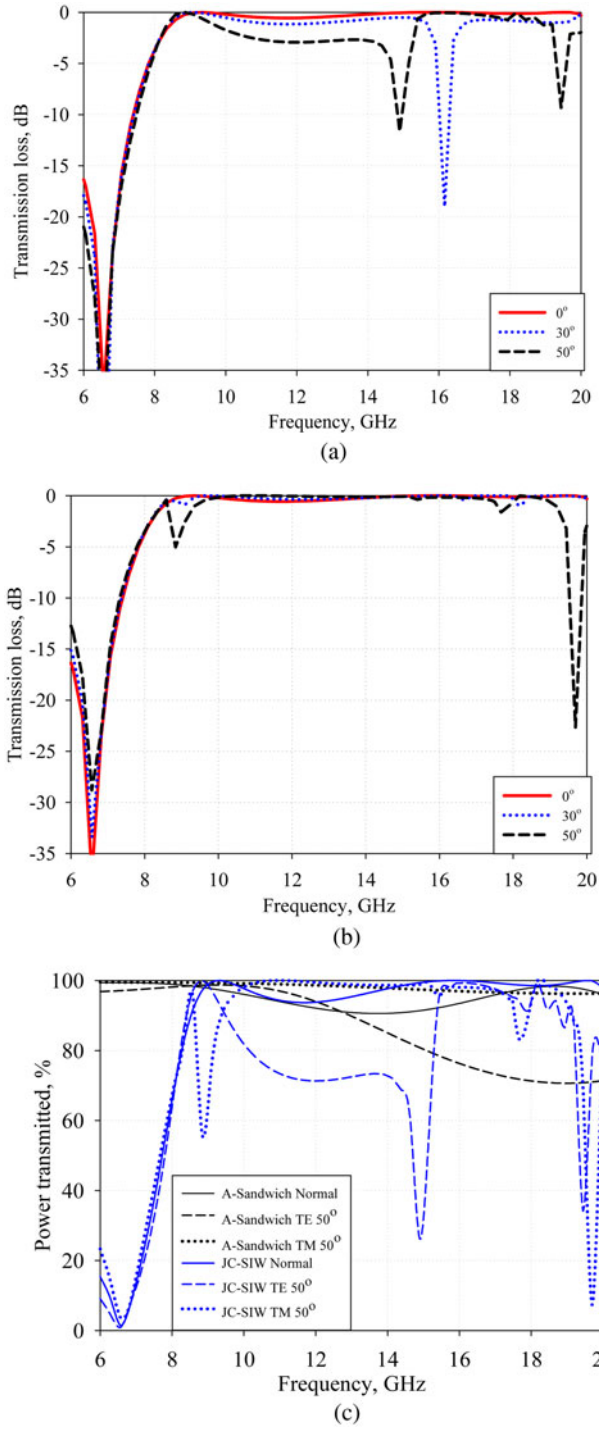


Fig. 5. Transmission characteristics of A-sandwich radome based on the proposed strongly coupled FSS at different incident angles: (a) TE polarization, (b) TM polarization, and (c) power transmission performance comparison of the proposed FSS radome structures with conventional radome (in %).

EM performance analysis of radome based on strongly coupled FSS element

In the view of radome application, EM performance of the proposed embodiment structure with strongly coupled JC FSS has been presented here. The response of the structure is monitored at different incident angles (normal, 30°, and 50°) for both TE and TM polarized incident wave and shown in Figs. 5(a) and 5(b). The results show a stable performance with reduced RCS at out of the band.

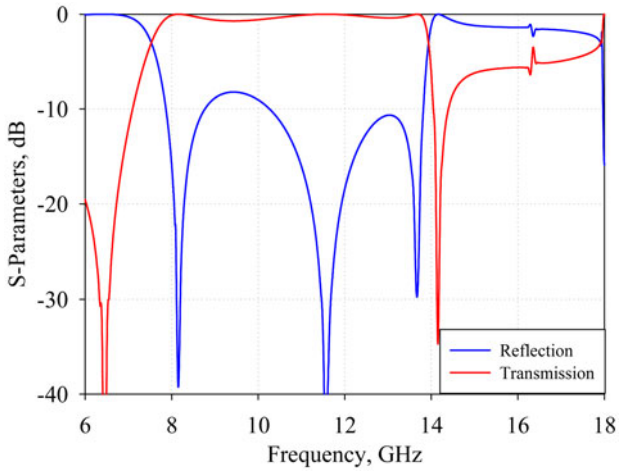


Fig. 6. Performance of the structure at an optimized thickness of 50° incident angle.

Power transmission efficiency

In this section, the power transmission efficiency of described radome wall configurations has been compared with that of convention A-sandwich structure. The power transmission efficiency of the structure at different incidence angles is shown in Fig. 5(c). The proposed structure shows superior performance at a normal incident angle. The suppression of out-band frequencies can be clearly observed here. The proposed structure suppresses all other bands before 8 GHz where many communication systems are operating at S and C bands. Also, after 20 GHz, where more space noise can be found. The maximum power transmission >90% is achieved up to 30° in the frequency range. As the angle of incidence increases, the performance of the structure starts degraded. It is worth to understand that the thickness is uniform in the above case. In general, the variable thickness of radome (VTR) is considered for better performance at a different angle of incidence. Hence the thickness of the radome wall has been optimized to achieve stable performance at higher incident angles. Also, the VTR structure is aerodynamically stable and distributes its weight along the aircraft body.

Thickness optimization

The stable performance of radome w.r.t the angle of incidence is the most desirable characteristics of radomes. Generally, the skin layer made the constant and variable thickness of core has been used in A-sandwich radome [2]. But, in the case of the proposed coupled-FSS core, the inter-elemental capacitance will decrease with increasing substrate height. Due to this, the resonance due to the core is shifted to lower frequency, which will change the operating frequency. To avoid this, the thickness of the skin has been optimized at 30–50° sector of incident angle. The radome section was divided into subsections for optimal performance at higher incident angles. Finally, the sector-wise optimized structure can be used to design the variable thickness monolithic radome and conformal structures. The optimum transmission performance has been observed at a skin thickness of 2.5 mm.

https://doi.org/10.1017/S1759078720000021 Published online by Cambridge University Press

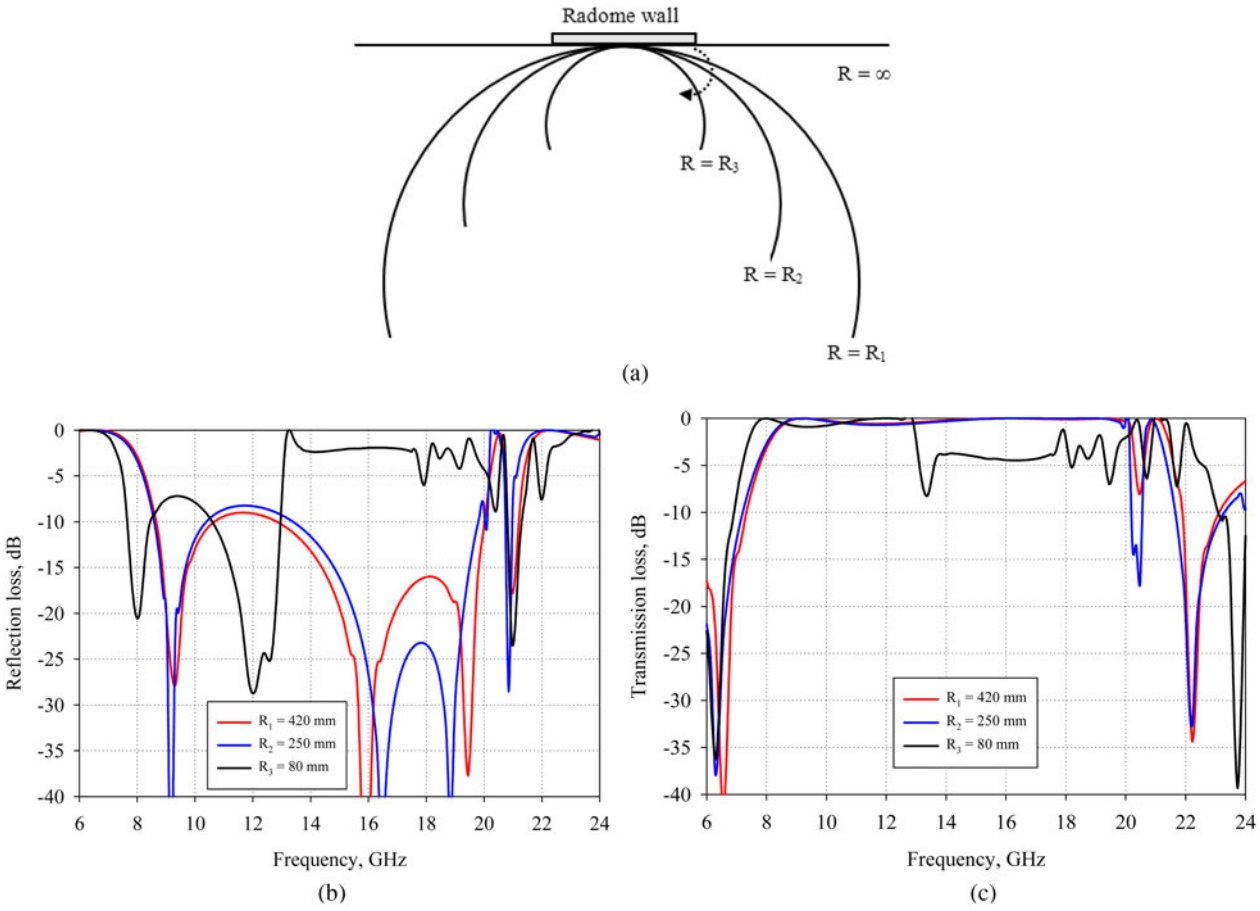


Fig. 7. Conformal analysis: (a) radius of conformal shape at different locations, (b) reflection loss, and (c) transmission loss.

Hence, the total thickness at 50° is 6.21 mm. For the above-optimized radome wall, the power transmission and reflection characteristics are studied and illustrated in Fig. 6. The response shows a very stable performance (>90%) from 8.0 to 13.8 GHz with strong reflections.

Conformal behavior

To study the practical behavior of the structure for radome application, the conformal analysis has been carried out in this section. Figure 7(a) shows the different bents in structure. The EM performance of the structure at different curved shapes is shown in Figs. 7(b) and 7(c). In the figure, at the diameter R3, the thickness of the structure is optimized to better transmission response at a 50° incident angle. At the diameter R_1, R_2 the structure shows a better than 90% passband characteristics up to 20 GHz in a conformal shape.

Experimental verification of proposed radome

To prove the efficacy of simulated results, the strongly coupled JC FSS structure presented in "Design aspects of strongly coupled FSS element" has been fabricated on a Rogers 4003C dielectric substrate with material characteristics $\varepsilon_r = 3.38 - j0.0091$ and thickness 0.81 mm using a surface machining process. An array of 14 × 16 cells (total elements = 224) elements is printed on a 135 mm × 155 mm sheet. The fabricated prototype is large enough to cover the mouth of the considered horn antenna. Then, tiny holes are drilled with a diameter of 0.5 mm with a spacing of 0.635 mm on the FSS elements and coated with a copper material with a 0.035 mm thickness to form metallic vias. The fabricated structure is used as the core of radome. Then, the total structure is sandwiched in between two FR-4 substrates with $\varepsilon_r = 4.3$ and $\tan\delta = 0.0017$ with a thickness of 2.0 mm each to develop the proposed radome wall configuration. To analyze the behavior of the proposed radome wall for practical application, the effect on the radiation pattern of the radome enclosed antenna has been studied. Figure 8(a) shows the simulation setup of the wideband horn antenna enclosed with the proposed radome wall. The radiation pattern of the radome wall enclosed radome has been tested in a fully shielded anechoic chamber shown in Fig. 8(b). The fabricated strongly coupled FSS based three-layer A-sandwich radome is shown in Fig. 8(c). The transmission characteristics of the fabricated prototype are tested in a fully shielded anechoic chamber. Two wideband horn antennas were used to transmit and receive EM energy. A vector network analyzer is connected to both transmit and receive antennas to analyze the transmission response. Both antennas were placed at a distance of 65 cm and the prototype is placed at the center. The standard thru, reflect, and line calibration is done to normalize the effect of the experimental setup. The measured transmission coefficient at normal and higher incidence angles for both TE and TM polarization is shown in Figs. 9(a) and 9(b) respectively. From the comparison, it is evident that the experimental

https://doi.org/10.1017/S1759078720000021 Published online by Cambridge University Press

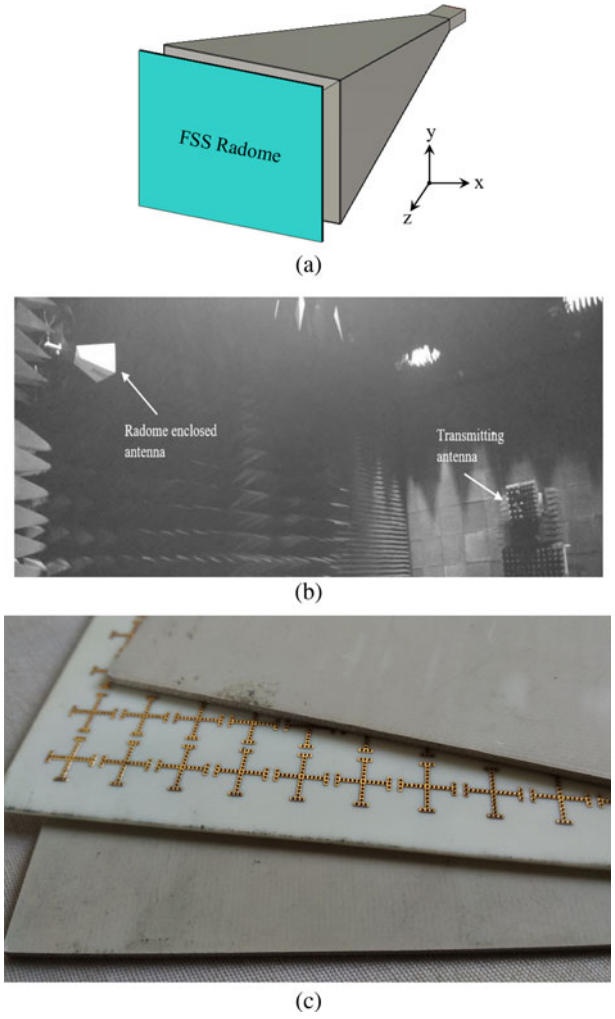


Fig. 8. Experimental verification: (a) simulation setup of the radome enclosed antenna, (b) anechoic chamber setup used to measure the radiation pattern, and (c) fabricated prototype of the three-layered radome wall with a strongly coupled FSS core.

results are well-matched with the estimated results with an error of ±5%. Furthermore, to test the effect of the radome wall on the radiation pattern of the antenna, the simulated radiation pattern in the transmission band of radome i.e., at 10.0, 11.00, and 12.0 GHz are compared with measured radiation patterns. The results shown in Figs. 10(a)–10(f) respectively are well matched and prove the feasibility of the proposed structure for radome application. Further, to examine the RCS performance of the planar slotted waveguide antenna (which is a modern antenna used in an active electrically scanned array radar in aircraft), the proposed radome wall is placed in front of the antenna and estimated its RCS response. The structure of the considered slotted waveguide antenna is shown in Fig. 11(a) [14], which is operating at a frequency of 9.5 GHz. It composed of 14 waveguides with 164 slots on whose two ends are perfectly matched in most of the practical conditions. The lengths of the four symmetrical rectangular waveguides are 306.12, 262.16, 218.2, and 130.28 mm, respectively. Two different sized slots have been carved on the top plane of waveguides. The dimensions of the slots are 13 mm × 1.2 mm and 13 mm × 2 mm, respectively. The separation between two adjacent slots is 8.7 mm in the *y*-direction and 0.3 mm in the *X*-direction. The monostatic RCS simulations are performed by the full-wave simulations (CST MWS). Figures 11(b) and 11(c) show the simulation results for the RCS of the considered antenna enclosed with the proposed radome wall at 9.5 GHz. The vertical polarization is in the *yz*-plane and horizontal polarization is in the *xy*-plane. At the same time, the simulation results are compared with the measured monostatic RCS of the unloaded planar slotted waveguide antenna. The results significantly improve the RCS performance in the operating region of the antenna. As shown in Fig. 11, the RCS values of the analyzed antenna are maximum for both polarizations at θ near 0°. This might be due to the fact that the plane of the antenna is considered as a perfect reflector surface at 0° incidence. Whereas, in the *xy*-plane (horizontal polarization) RCS is relatively high at $\pm\theta = 60^{\circ}$ and very high at the incidence of $\pm\theta = 45^{\circ}$ in the *yz*-plane (vertical polarization). The instance of the *xy*-plane is better than *yz*-polarization. The effect is mainly because of EM

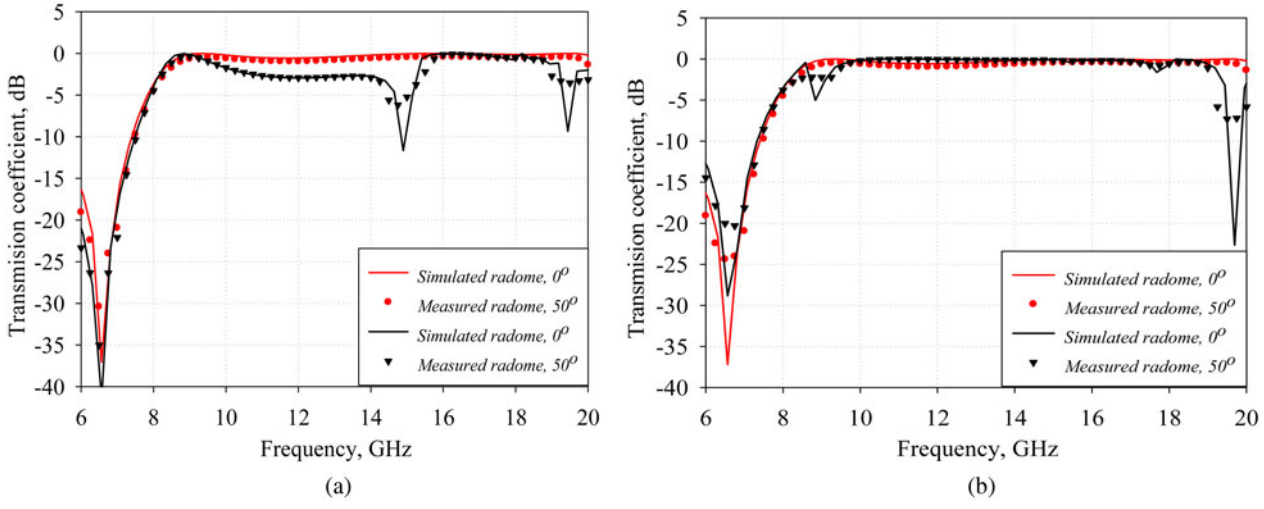


Fig. 9. Comparison of the measured transmission coefficient: (a) TE at 0 and 50° and (b) TM at 0 and 50°.

https://doi.org/10.1017/S1759078720000021 Published online by Cambridge University Press

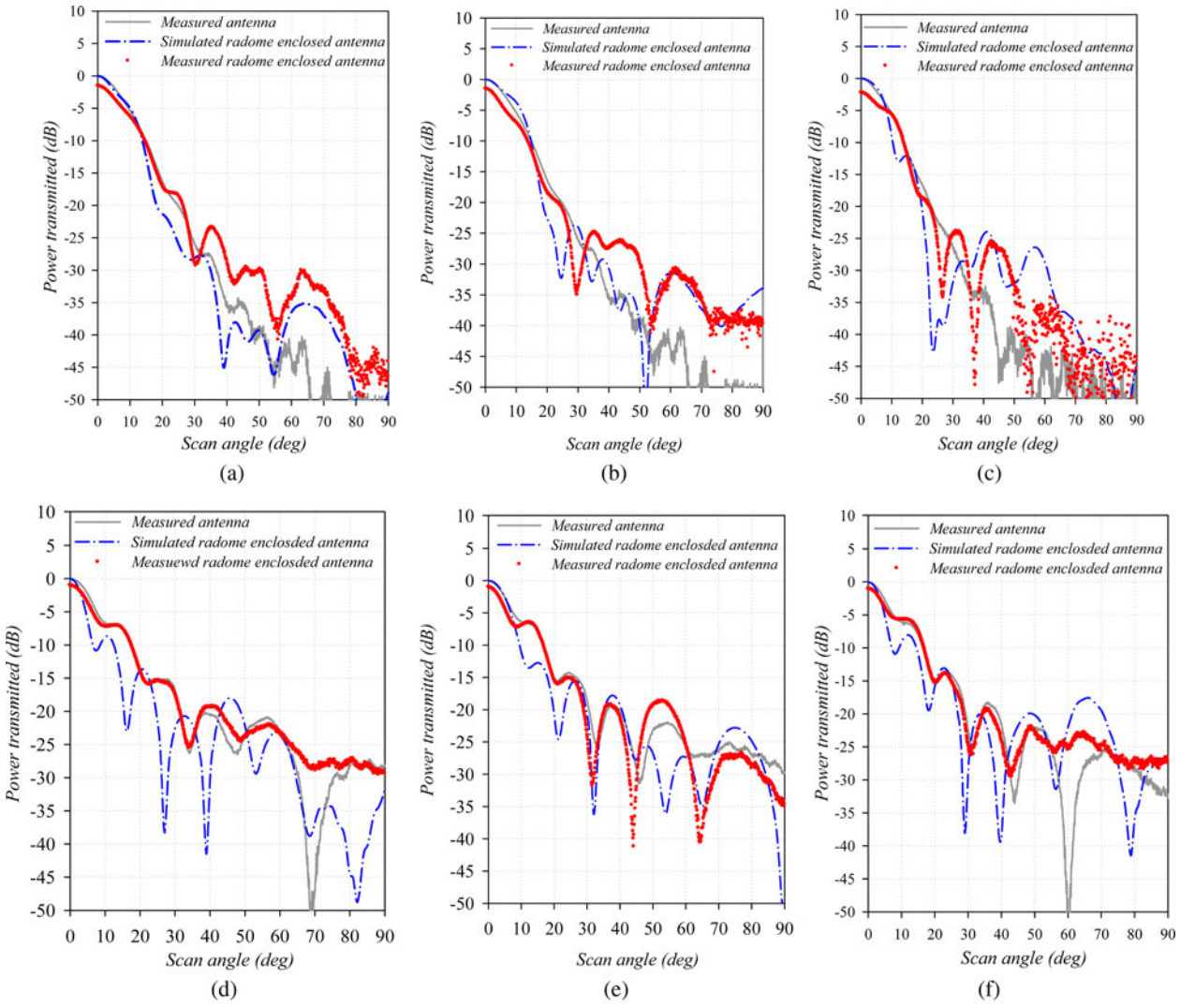


Fig. 10. Radiation characteristics of the proposed structure enclosed to a horn antenna: (a) simulation set up, radiation pattern, (b) E-plane at 10 GHz, (c) H-plane at 10 GHz, (d) E-plane at 11 GHz, (e) H-plane at 11 GHz, (f) E-plane at 12 GHz, and (g) H-plane at 12 GHz.

wave reflection of the slotted structure in the longitudinal direction of the slots is being normal to the direction of wave propagation when vertical polarization occurring. It is observed that the RCS values of the considered antenna have been improved significantly when covered with proposed radome. Remarkable reduction in crest values of RCS is found in the radome enclosed antenna.

Though the proposed radome improves the RCS performance, exhibits very good transmission, and radiation characteristics, its presence may generate perturbations with an antenna, may introduce slight error, degrades polarization purity, and may increase the side lobe power. However, the proposed radome is superior in many performance characteristics of conventional dielectric radomes. Further, parameters of the proposed radome can be optimized in future studies.

Conclusion

The A-sandwich radome wall configuration using a novel strongly coupled FSS element using metallic vias technology has been demonstrated. The issues related to the design of the FSS element based on coupled vias technology have been discussed. Further, the performance of the sandwiched structure has been analyzed with anti-static and anti-erosion radome painted on top layers. The structure exhibits very good band-pass characteristics (>90%) in X and Ku-bands at a normal impinging angle with sharp roll-off from 8.5 to 17.5 GHz. To show the efficacy of the proposed structure, transmission loss has been compared with that of conventional A-sandwich radomes at 0°, 50° incidence angle for both TE and TM polarization. Conformal analysis of the unit cell has been carrying out and sector-wise thickness optimization was performed to analyze the structure for nosecone radome application. The transmission and radiation characteristics of the radome wall are experimentally verified and results prove completely transparent in the region. Further, the simulated RCS of the structure on a slotted waveguide antenna proves the improved RCS performance in the passband.

Acknowledgement. The authors would like to thank Dr. D. C. Pande, distinguished scientist, DRDO-LRDE, Bangalore and Dr. Shiv Narayan, Sr. Scientist, Center for Electromagnetics (CEM), CSIR-NAL, Bangalore for their useful discussions and technical support.

https://doi.org/10.1017/S1759078720000021 Published online by Cambridge University Press

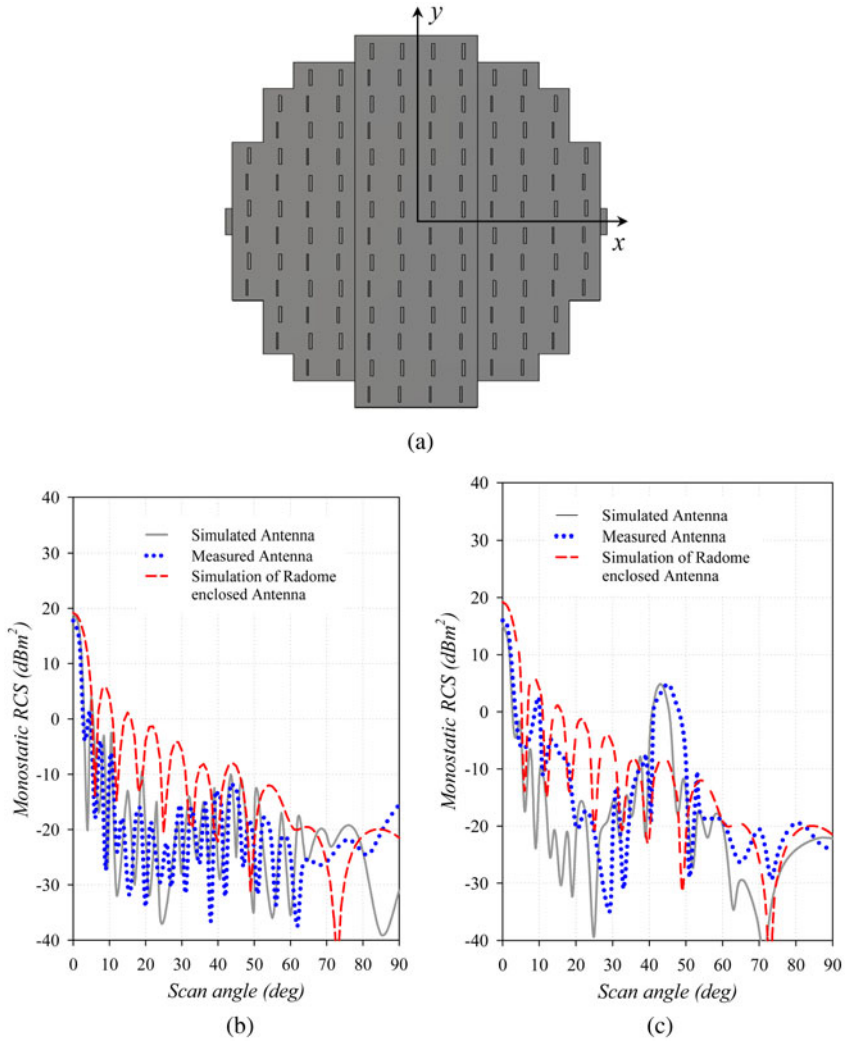


Fig. 11. Monostatic RCS of the covering radome wall on the slotted waveguide antenna at 9.5 GHz: (a) slotted waveguide antenna, (b) horizontal polarization (*xy*-plane), and (c) vertical polarization (*yz*-plane).

References

1. **(1975)** ***Military specification: General specification for radomes*, MIL-R-7705A.**
2. **Yazeen PSM, Vinisha CV, Vandana S, Suprava M and Nair RU** (2017) Electromagnetic performance analysis of graded dielectric inhomogeneous streamlined airborne radome. *IEEE Transactions on Antennas and Propagation* **65**, 2718–2723.
3. **Kozakoff DJ** (2010) *Analysis of Radome Enclosed Antennas*. Norwood, MA, USA: Artech House.
4. **Nair RU and Jha RM** (2014) Electromagnetic design and performance analysis of airborne radomes: trends and perspectives. *IEEE Antennas and Propagation Magazine* **56**, 276–298.
5. **Narayan S and Jha RM** (2015) Electromagnetic techniques and design strategies for FSS structure applications [Antenna Applications Corner]. *IEEE Antennas and Propagation Magazine* **57**, 135–158.
6. **Xu W, Duan B, Li P, Yang G and Qiu Y** (2017) Integrated optimum design of metal space frame radomes with variable size members involving electromagnetic and structural analysis. *IET Microwaves, Antennas & Propagation* **11**, 1565–1571.
7. **Moccia M, Castaldi G, D'Alterio G, Feo M, Vitiello R and Galdi V** (2017) Transformation-optics-based design of a metamaterial radome for extending the scanning angle of a phased-array antenna. *IEEE Journal on Multiscale and Multiphysics Computational Techniques* **2**, 159–167.
8. **Xu W, Duan BY, Li P and Qiu Y** (2017) Study on the electromagnetic performance of inhomogeneous radomes for airborne applications – part II: the overall comparison with variable thickness radomes. *IEEE Transactions on Antennas and Propagation* **65**, 3175–3183.
9. **Xu W, Duan BY, Li P and Qiu Y** (2017) Study on the electromagnetic performance of inhomogeneous radomes for airborne applications – Part I: characteristics of phase distortion and boresight error. *IEEE Transactions on Antennas and Propagation* **65**, 3162–3174.
10. **Munk BA** (2000) *Frequency Selective Surfaces: Theory and Design*. New York: Wiley.
11. **Lee J, Yoo M and Lim S** (2015) A study of ultra-thin single layer frequency selective surface microwave absorbers with three different bandwidths using double resonance. *IEEE Transactions on Antennas and Propagation* **63**, 221–230.
12. **Raytheon Company, Waltham**, Cannon BL and Jordan JW. "Multiband-band-pass, dual polarization radome with Embedded gridded structures", United State patent (US 2014/0118217 A1).
13. **Narayan S, Prasad K, Nair RU and Jha RM** (2012) A novel EM analysis of double-layered thick FSS based on MM-GSM technique for radome application. *Progress In Electromagnetics Research Letters* **25**, 53–62.
14. **Chen H, Hou X and Deng L** (2009) Design of frequency-selective surfaces radome for a planar slotted waveguide antenna. *IEEE Antennas and Wireless Propagation Letters* **8**, 1231–1233.
15. **Xu F, Jiang X and Wu K** (2008) Efficient and accurate design of substrate-integrated waveguide circuits synthesised with metallic via-slot arrays. *IET Microwaves, Antennas & Propagation* **2**, 188–193.
16. **Luo GQ, Hong W, Tang HJ and Wu K** (2006) High performance frequency selective surface using cascading substrate integrated

https://doi.org/10.1017/S1759078720000021 Published online by Cambridge University Press

waveguide cavities. *IEEE Microwave and Wireless Components Letters* **16**, 648–650.
17. **Krushna Kanth V and Raghavan S** (2018) Ultrathin design and implementation of planar and conformal polarisation rotating frequency selective surface based on SIW technology. *IET Microwaves, Antennas & Propagation* **12**, 1939–1947.
18. **Krushna Kanth V and Raghavan S** (2019) Design and implementation of 2.5D frequency-selective surface based on substrate-integrated waveguide technology. *International Journal of Microwave and Wireless Technologies* **11**, 255–267.
19. **Cary RHJ** (1982) Radomes. In Rudge AW, Milne K, Olver AD and Knight P (eds), *the Handbook of Antenna Design*. London, UK: Peter Peregrinus. (Chapter. 14, pp. 457–550).
20. **Pozar DM** (2012) *Microwave Engineering*, 4th Edn. Inc., New York, USA: Johm Wiley & sons, Inc.
21. **Wu JH, Scholvin J, del Alamo JA and Jenkins KA** (2001) A Faraday cage isolation structure for substrate crosstalk suppression. *IEEE Microwave and Wireless Components Letters* **11**, 410–412.
22. **Xu RR, Zong ZY, Yang G and Wu W** (2008) Loaded frequency selective surfaces using substrate integrated waveguide technology. *Microwave and Optical Technology Letters* **50**, Chapter. 14.
23. **Anderson I** (1975) On the theory of self-resonant grids. *The Bell System Technical Journal* **54**, 1725–1731.
24. **Winkler SA, Hong W, Bozzi M and Wu K** (2010) Polarization rotating frequency selective surface based on substrate integrated waveguide technology. *IEEE Transactions on Antennas and Propagation* **58**, 1202–1213.
25. **Zhang H, Meng R, Xia Z and Zhu Q** (2014) A novel substrate integrated waveguide slot antenna with high power-handling capacity. *IEEE Antennas and Propagation Society International Symposium* (APSURSI), Memphis, TN, 1037–1038.
26. **Parment F, Ghiotto A, Vuong TP, Duchamp JM and Wu K** (2015) Air-filled substrate integrated waveguide for low-loss and high power-handling millimeter-wave substrate integrated circuits. *IEEE Transactions on Microwave Theory and Techniques* **63**, 1228–1238.
27. **Munk BA, Luebbers R and Mentzer CA** (1971) Breakdown of periodic surfaces at microwave frequencies', *ElectroScience Lab., Dept. Elect. Eng., Ohio State Univ., Columbus, OH, Tech. Rep*, 2989-1.
28. **Marcuvitz N** (1951) *Waveguide Handbook*. New York: McGraw-Hill



KK Varikuntla was received his B.Tech degree from JNTUA, Andhra Pradesh, India, in 2012 and M. Tech. degree in Electronics Engineering from Pondicherry University, India, in 2015. He was with the Centre for Electromagnetics of CSIR-National Aerospace Laboratories (CSIR-NAL), Bangalore, India for a period of one year as Project Assistant-III. He is currently a research scholar at the Department of Electronics and Communication Engineering, National Institute of Technology Tiruchirappalli, India. He is a student member of IEEE, student member of European Microwave Association (EuMA), student member of IEEE Microwave Theory & Techniques Society (MTT-S), IEEE Antenna Propagation Society (AP-S), IEEE Electromagnetic Compatibility Society (EMC-S), IEEE Electronics Packaging Society (EP-S), IEEE Instrumentation and Measurement Society (IM-S), & IEEE Signal Processing Society (SP-S). Also, a Corresponding Member of the International Union of Radio Science (URSI). To his credit, he published more than 20 technical papers and co-authored springer brief. Krushna Kanth won the first prize (individual category) in DRDO Dare-to-Dream innovation contest for the year 2019. Also, four best paper awards in various conferences. His particular focus areas are design and analysis of frequency selective surfaces (FSS) towards the realization of high-performance stealth radome, polarizers, RAS/RAM, low RCS antenna, RCS field computations, etc., to the aerospace/defence applications. Also, the substrate-integrated waveguide technology, metasurfaces, microwave integrated circuits, filters, and antenna design.



S Raghavan (M'98–SM'05) is a senior professor at the Department of Electronics and Communication Engineering, National Institute of Technology Tiruchirappalli, India. He has awarded Ph.D. degree from IIT-Delhi, India in 2001. He is having 35 years of educational activity and research experience in the area of RF and Microwave. He is a recipient of IETE-Smt Ranjana Pal Memorial Award 2019. The Best Teacher Award for the year 2007–08, Best Faculty Award for Electrical and Electronics division (P. K. Das Memorial Award) for the year 2010–11, Life Time Achievement in Microwave Engineering, Honorary Fellowship of Ancient Sciences and Archeological Society of India. He received IETE Smt Ranjana Pal award in 2019. He is a senior member in IEEE-MTT, EMBS, and CSI. Fellow in IETE, FIE, BESI, and ATMS and Life Member in ISTE, ISSS, SEMCE, MRSI, IATLIS, ILS, NPC, IAMI, BMES, SBAO, STERM, and ASI. His specialization is Microwave Engineering and Microwave integrated circuits. He was the short term Visiting Fellow at California State University, North Ridge (CSUN), USA. Dr. Raghavan has authored or co-authored more than 500 scientific research papers and technical reports. He has been a reviewer for many technical journals, such as IEEE Microwave Theory and Techniques, IET Microwave, Antenna and Propagation, AUE, Journal of Electronics and Telecommunication Engineering, Institution of Engineers, PIERS, etc. His research interest includes Microwave integrated circuits, Biological effects of Microwaves, Computer-Aided Design of MICS, Biomedical Informatics, Metamaterials/FSS, Bio-MEMS, RF MEMS, Fractal Antennas, MIC Antenna, Metamaterial Antenna, and Substrate Integrated Waveguide.

https://doi.org/10.1017/S1759078720000021 Published online by Cambridge University Press